Tuning Aryl, Hydrazine Radical Cation Electronic Interactions Using Substitutent Effects

Guadalupe Valverde-Aguilar, Xianghuai Wang, Edward Plummer, Jenny V. Lockard, and Jeffrey I. Zink*

Department of Chemistry and Biochemistry, University of California Los Angeles, California 90095

Yun Luo, Michael N. Weaver, and Stephen F. Nelsen*

Department of Chemistry, University of Wisconsin, 1101 University Avenue, Madison, Wisconsin 53706-1396

Received: December 21, 2007; Revised Manuscript Received: May 27, 2008

Absorption spectra for 2,3-diaryl-2,3-diazabicyclo[2.2.2]octane radical cations (**2(X)**$^{\bullet+}$) and for their monoaryl analogues 2-*tert*-butyl-3-aryl-2,3-diazabicyclo[2.2.2]octane radical cations (**1(X)**$^{\bullet+}$) having para chloro, bromo, iodo, cyano, phenyl, and nitro substituents are reported and compared with those for the previously reported **1**- and **2(H)**$^{\bullet+}$ and **1**- and **2(OMe)**$^{\bullet+}$. The calculated geometries and optical absorption spectra for **2(Cl)**$^{\bullet+}$ demonstrate that *p*-C_6H_4Cl lies between *p*-C_6H_4OMe and C_6H_5 in its ability to stabilize the lowest energy optical transition of the radical cation, which involves electron donation from the aryl groups toward the $\pi^*(NN)^+$-centered singly occupied molecular orbital of **2(X)**$^{\bullet+}$. Resonance Raman spectral determination of the reorganization energy for their lowest energy transitions (λ_v^{sym}) increase in the same order, having values of 1420, 5300, and 6000 cm^{-1} for X = H, Cl, and OMe, respectively. A neighboring orbital analysis using Koopmans-based calculations of relative orbital energies indicates that the diabatic aryl π-centered molecular orbital that interacts with the dinitrogen π system lies closest in energy to the bonding π(NN)-centered orbital and has an electronic coupling with it of about 9200 ± 600 cm^{-1}, which does not vary regularly with electron donating power of the **X** substituent.

Introduction

This work principally concerns the optical spectra of the radical cations of monoaryl and diaryl 2,3-diazabicyclo[2.2.2]octanes, **1(X)**$^{\bullet+}$ and **2(X)**$^{\bullet+}$. For convenience their designation includes their aryl substituents. All the

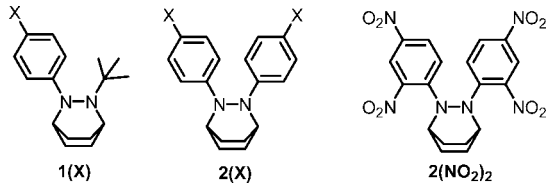

compounds considered have p-substituted phenyl substituents, except for the 2,4-dinitrocompound shown as **2(NO$_2$)$_2$**. These compounds show lowest energy optical spectrum absorption bands that correspond to **Ar**-to-(**NN**)$^{\bullet+}$ electron transfer, and their transition energies are sensitive to the substituents **X**. Hydrazine radical cations are unusual delocalized (Robin-Day Class III)[1] mixed valence (MV) compounds that lack a bridge. They have their disubstituted amino charge-bearing units directly attached by the NN σ bond, and an NN π system having a pair of π electrons, and one π^* electron.[2] In the case of **2(X)**$^{\bullet+}$ some charge and spin leaks onto the aryl groups but most resides on the hydrazine 3e-π system. We believe that Creutz first pointed out that the two-state model requires that the transition energy for a Class III MV compound is $2H_{ab}$,[3] where H_{ab} is the electronic coupling between the **M** groups. Many theoretical investigations of H_{ab} have relied upon this prediction of the two-state model, usually with reference to the pioneering work of Larsson and co-workers.[4] Three reviews of IV compounds that have H_{ab} near $\lambda/2$, so they are near the Class II/Class III borderline and have very fast electron transfer, have appeared since 2000,[5–7] all employing the two-state model. A principal theme of the present work is that the two-state model should not be applied without alteration to **2(X)**$^{\bullet+}$ or other delocalized MV compounds. In a previous absorption, fluorescence, and resonance Raman study of a 1,4-dihydrazine-substituted durene diradical dication,[8] we pointed out that it does not have a single excited state centered at 0.5 in a Marcus−Hush diagram that the two-state model predicts, because the excited state is split by the fact that either hydrazine group could participate in superexchange electron transfer, so this compound has a Marcus−Hush two-state diagram for its lowest excited state. It is not at an MV oxidation level because each hydrazine is at the +1 oxidation level. A somewhat analogous split excited state was found to be exhibited by the MV monocation **2(H)**$^{\bullet+}$,[9] although the weaker higher energy component of its excited state absorption was not well resolved from other, higher energy, absorptions. The higher energy component of the split excited state was larger and its resolution better for the anisyl-substituted compound **2(OMe)**$^{\bullet+}$,[10] which allowed a resonance Raman spectroscopy study showing that the excited state coupling affects the absorption band widths for the two components in a manner that may be successfully calculated from the observed Raman intensities and excitation profiles. In this work we consider the trends in excited state splitting, reorganization energy, and electronic coupling that are caused by tuning the energy of the aryl group molecular orbital (MO) relative to those of

* Corresponding authors.

10.1021/jp7120005 CCC: $40.75
Published on Web 07/23/2008

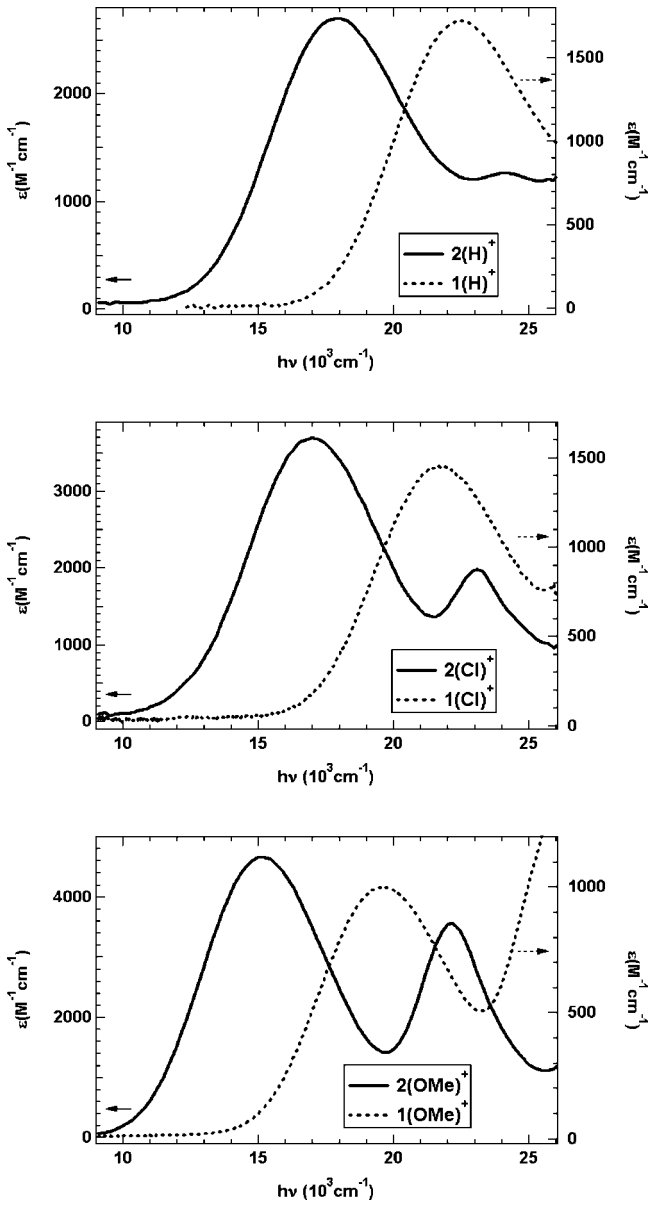

Figure 1. Pairwise comparison of absorption spectra of **2(X)**$^{\bullet+}$ and **1(X)**$^{\bullet+}$ in acetonitrile for **H**, (top panel) **Cl**, (middle panel) and **OMe**-substitution (bottom panel).

the π and $\pi^*(NN)^+$ MOs by changing the para substituents on the aryl rings.

Results and Discussion: Redox Potentials and Optical Absorption Spectra

The absorption spectra of the mono- and diaryl **H**, **Cl**, and **OMe**-substituted compounds are compared in Figure 1, where it is seen that substantial lowering of the first transition energies and increase of their intensity occur upon substitution with electron-releasing substituents for the diaryl compounds, and that the higher energy component of the split absorption, which has been discussed in detail for the parent,[8] becomes more distinct. The spectra of the halogen-substituted radical cations are compared with the cyano-substituted compound in Figure 2. The best resolution of the excited state absorptions is shown by **2(Cl)**$^{\bullet+}$, which was selected for a resonance Raman study in this work. See the Supporting Information for the spectra of **2(Ph)**$^{\bullet+}$, **2(NO$_2$)**$^{\bullet+}$, and **2(NO$_2$)$_2$**$^{\bullet+}$. Although **2(Ph)**$^+$ has the lowest energy absorption maximum of the monosubstituted

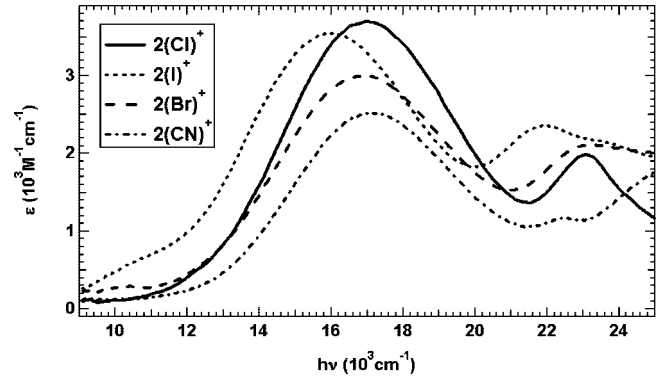

Figure 2. Comparison of the spectra of **2(I)**$^{\bullet+}$, **2(Br)**$^{\bullet+}$, **2(Cl)**$^{\bullet+}$, and **2(CN)**$^{\bullet+}$.

compounds, the second component of its lowest energy band is rather broad and is not very well resolved. The dinitrophenyl-substituted compound, which was prepared unintentionally when **2(H)** was nitrated under conditions that were too harsh to isolate **2(NO$_2$)**, has the lowest absorption maximum of all the **2(X)**$^+$ studied. Its ortho substituents cause considerably more twisting at the N,aryl bonds than in the other cases, and its spectrum is rather different from that of the other compounds and will not be discussed further here. Increased higher energy absorption by both nitro-substituted compounds obscures the region where the second component of the first band would be expected.

The optical data for **1(X)**$^{\bullet+}$ and **2(X)**$^{\bullet+}$ and formal oxidation potentials ($E^{\circ\prime}$) for **2(X)** are summarized in Table 1. The ε values are less certain for the less stable monoaryl compounds; they were calculated assuming no decomposition upon oxidation of the neutral compound, and the monoaryl radical cations are clearly less stable than the diaryl ones. Table 2 shows calculated geometrical information, using the UB3LYP/6-31G* level of theory. The parameters that change significantly with the electron-releasing ability of the substitutents are the lone pair, aryl carbon p orbital twist angle at the N,aryl bond (ϕ_{CN}), the

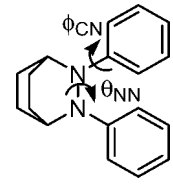

lone pair, lone pair twist at the NN bond (θ_{NN}) and the pyramidality at the hydrazine nitrogens (we use $\Delta\alpha_{av}$, the difference between the 120° average heavy atom bond angle at nitrogen for a planar N atom and the observed value). As the substituents become less electron releasing and can accept less positive charge from the $(NN)^+$ unit, more twist occurs at the CN bonds, which is accompanied by less twist at the NN bond (so θ_{NN} becomes smaller: 180° corresponds to no twist, and 90° to the greatest possible twist at the $(NN)^+$ bond, which of course cannot be achieved because of the bicyclic ring attached to the nitrogens), and more flattening at nitrogen ($\Delta\alpha_{av}$ becomes smaller). The 2,4-dinitro compound, which has increased CN twist for steric as well as electronic reasons, has more pyramidality at the hydrazine nitrogens than expected from the trend of the compounds that lack ortho substituents, because the more twisted aryl groups cannot interact as much with the $(NN)^{\bullet+}$ group.

p-Chlorophenyl is often a poorer electron donor than phenyl. For example, *p*-chlorobenzoic acid is slightly more acidic than

TABLE 1: Absorption Spectra and Formal Potentials for 2(X)$^{\bullet+}$ and Absorption Spectra for 1(X)$^{\bullet+}$

2(X)$^{\bullet+}$	$E_{a1,max}$, cm^{-1}	$\varepsilon_{1,max}$, M^{-1}cm^{-1}	$E_{a2,max}$, cm^{-1}	$\varepsilon_{2,max}$, M^{-1}cm^{-1}	$E^{\circ\prime}V^{a}$ (ΔE^{pp}, mV)	1(X)$^{\bullet+}$	$E_{a1,max}$, cm^{-1}	$\varepsilon_{1,max}$, M^{-1}cm^{-1}
Ph	14800	3400	20000	2150	0.51 (74)	**Ph**	19500	2000
MeO	15200	4700	22200	3600	0.31 (76)	**MeO**	19600	1800
I	16100	3300	21900	2250	0.62 (73)	**I**	21000	1700
Br	16800	3000	23000	2200	0.63 (80)	**Br**	21700	1700
Cl	17000	3700	23000	2000	0.56 (80)	**Cl**	21700	1500
H	18000	2400	24200	1300	0.49 (80)	**H**	22500	1700
CN	17200	2500	22500	1200	0.87 (76)	**CN**	*b*	
NO$_2$	17300	2500			0.94 (76)	**NO$_2$**	*b*	
(NO$_2$)$_2$	14200	7550	16600	2700	0.73 (72)			

[a] In acetonitrile containing 0.1 M. Bu_4NClO_4. Potentials measured versus ferrocene as an internal standard and reported versus SCE, using +0.395 as the $E^{\circ\prime}$ of ferrocene. [b] Not studied because it decomposed too rapidly.

TABLE 2: UB3LYP/6-31G* Optimized Geometries for 2(X)$^{\bullet+}$ and 1(X)$^{\bullet+}$

2(X)$^{\bullet+}$	θ_{NN}, deg	ϕ_{CN}, deg	$\Delta\alpha_{av}$, deg	1(X)$^{\bullet+}$	θ_{NN}, deg	ϕ_{CN}, deg	$\Delta\alpha_{av}$ NAr
Me$_2$N	144.0	36.4	2.25	**Me$_2$N**	140.0	39.7	2.49
Ph	148.0	38.2	1.62	**Ph**	145.5	52.2	2.58
MeO	148.9	39.5	1.78	**MeO**	146.1	50.8	2.51
Br	151.0	41.4	1.58	**Br**	145.5	53.3	2.61
Cl	150.9	41.3	1.60	**Cl**	146.8	52.6	2.61
H	152.5	42.6	1.53	**H**	147.2	53.6	2.61
CN	152.1	41.3	1.48	**CN**	147.0	53.6	2.58
NO$_2$	153.4	42.4	1.41	**NO$_2$**	147.6	53.5	2.56
***o,p*-(NO$_2$)$_2$**	156.4	53.7	1.94	***o,p*-(NO$_2$)$_2$**	149.9	57.6	1.12

benzoic acid, causing the *p*-Cl substitutent to have a positive Hammett σ value (that for *p*-H is defined as zero). As expected from these σ values, it is harder to remove an electron from **2(Cl)** than from **2(H)** or **2(OMe)**, by 1.6 and 5.8 kcal/mol respectively according to the formal oxidation potentials in Table 1. Nevertheless, from the structural changes of Table 2 it is clear that *p*-C_6H_4Cl lies between *p*-C_6H_4OMe and C_6H_5 in its ability to stabilize the $\pi(NN)^+$ unit of **2(X)**$^{\bullet+}$; that is, *p*-Cl has a slightly negative σ, the same sign as *p*-MeO, for donation of charge to $\pi(NN)^+$. There is a fine balance between the importance of inductive and resonance interactions in various structural situations that leads to the change in whether C_6H_5 or C_6H_4Hal is the better electron donor.[11] It is, in fact, not unusual for *p*-Cl and *p*-OMe substituents to have the same sign of σ for interaction with radical centers. For example, as Adam and co-workers discussed in detail,[12] both *p*-Cl and *p*-MeO lower the α-CH_2 ESR splitting of benzyl radicals, and both increase the rates for allylic rearrangement of 1-methylene-2-ary1−3,3-dimethyl-cyclopropanes to 1-isopropylidene-2-arylcyclopropanes, the rates of decomposition of bis(arylmethyl)mercury, and the rates of dimerization of aryltrifluoroethylenes, all of which have been used to define radical "$\sigma^{\bullet}$" scales. However, other cases of aryls attached to radical-bearing centers have opposite signs for substituent effects of *p*-Cl and *p*-MeO, which is expected when charge polarization effects predominate.[13] For the experimental result we have found that is most similar to that being discussed, Claridge and Fischer showed that the optical absorption bands for substituted benzyl radicals are shifted to lower energy by *p*-Cl, *p*-MeO, and *p*-Me substituents, with the lowest energy absorption band being the most sensitive.[14] The fact that **2(Ph)**$^{\bullet+}$ has the lowest E_{a1} of the compounds studied demonstrates that it is not simply inductive "electron donating ability" that is important for lowering the transition energy. The ability to delocalize the positive charge transferred to the aryl groups is also important.

Resonance Raman Study of 2(Cl)$^{\bullet+}$

The analysis of resonance Raman intensities is a powerful tool for determining the distortions that molecules undergo upon excitation and for experimentally probing excited state potential surfaces.[15–24] Resonance Raman excitation profiles are especially useful when electronic absorption and emission spectra are unstructured, as for **2(X)**$^{\bullet+}$. Although the electronic spectra of large molecules in condensed media contain information about all of the normal modes of the molecule whose potential surface minima are displaced from the minimum of the ground electronic state, the spectra of molecules with many displaced normal modes are frequently so congested that only an unresolved envelope or ill-resolved shoulders are observed. In contrast, *rR* profiles give information about individual modes because the excited state information is "filtered" through the specific normal mode being examined. *rR* excitation profiles are a collection of the *rR* intensities of each mode at various excitation wavelengths. To construct the experimental excitation profiles, spectra are taken at various excitation wavelengths in resonance with the absorption band of interest. An internal standard, a molecule that does not absorb at the excitation wavelength, is used to obtain the intensity of each vibrational mode relative to that of the standard. The normal modes of vibration that are the most highly distorted are identified and have been assigned in this work using UB3LYP/6-31G* calculations. The *rR* intensities and excitation profiles were calculated by using time-dependent theory and the excited state distortions Δ obtained by fitting the Raman spectra, their excitation profiles, and the electronic absorption spectrum using parabolic potential energy surfaces. See the Supporting Information for Raman spectra of **2(Cl)**$^{\bullet+}$ obtained at excitation wavelengths of 568.2 and 488.0 nm. The majority of the modes decrease in intensity when the excitation frequency is changed from 568.2 to 488.0 nm excitation.

Plots of the resonance Raman excitation profiles, including their error bars, are given in Figure 3 for the bands with the biggest distortions (those with intensities at least 10% of the largest, the 465 cm^{-1} mode in the in the 568.2 nm *rR* spectrum). The solvent, acetonitrile, was used as the internal standard. The spectra that were used to construct the profiles were obtained using 676.4, 647.1, 568.2, 514.5, and 482.5 nm excitations (14784, 15453, 17599, 19436, and 20725 cm^{-1}, respectively),

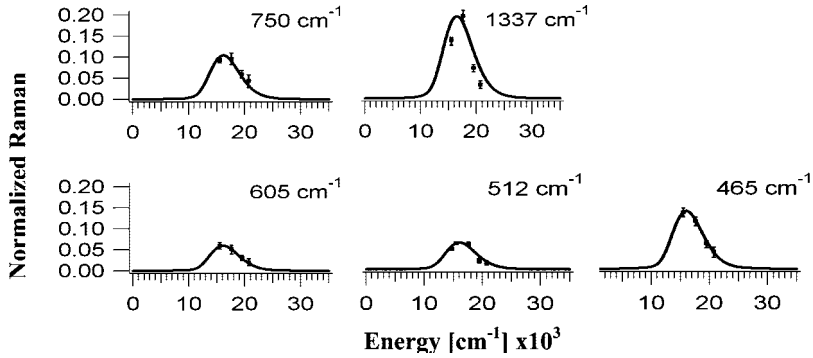

Figure 3. Resonance Raman excitation profiles of the five most enhanced normal modes of **2(Cl)**$^+$. The experimental points are shown with experimental uncertainty bars, and the calculated fits shown as solid lines. All experimental and calculated plots are shown on the same scale.

TABLE 3: Raman Frequencies, Distortions and Assignments of 2(Cl)$^+$

ω_q[a]	I_{568}/I_{ref}	Δ_q	δ_q, Å	λ_q^{sym} [a]	ω_{calc}[a,b]	description
465	0.110	1.97	0.31	902	467	N bend
512	0.059	1.31	0.19	439	489	N bend
605	0.052	1.04	0.12	327	602	N bend
630	0.031	0.77	0.10	187	641	in plane
705	0.016	0.49	0.05	85	684	aryl bend
750	0.096	1.14	0.13	487	750	ring breathing
1097	0.027	0.41	0.04	92	1128	NN stretch
1182	0.109	0.77	0.05	350	1192	CN st. (CNNC?)
1202	0.090	0.69	0.05	286	1213	in plane CN str., CH wag
1268	0.130	0.78	0.05	386	1242	N bend. CN stretch
1284	0.040	0.43	0.03	119	1277	NN stretch
1337	0.197	0.92	0.09	566	1358	NN stretch
1399	0.070	0.52	0.05	189	1375	N bend. CN stretch
1423	0.168	0.79	0.07	444	1404	NN stretch
1581	0.186	0.75	0.10	445	1590	aryl ring deformation

[a] Unit, cm^{-1}. [b] From a UB3LYP/6-31G* calculation.

which are all within the low energy band of **2(Cl)**$^{\bullet+}$. The intensities of the *rR* bands and their excitation profiles were calculated (see Experimental Section), and these results are shown as the solid lines in Figure 3. The variable parameters that are used in the calculation are the mode energies (ω_q) and distortions (Δ_q), shown in Table 3, and the damping factor (Γ), for which a value of 700 cm^{-1} gave the best fit. The intensity of each excitation profile in Figure 3 is roughly proportional to $\omega_q^2\Delta_q^2$. In Table 3 ω_q is the observed energy of the vibrational mode in cm^{-1}, I_{568}/I_{ref} is the ratio of intensities of the 568.2 nm (17599 cm^{-1}) Raman spectrum to the acetonitrile standard peak at 920 cm^{-1}, Δ_q is the dimensionless distortion along the normal coordinate, δ_q and λ_q^{sym} are discussed below, and ω_{calc} is the normal mode energy calculated at the B3LYP/6-31G* level. The mode with the largest distortion is the lowest energy N bend at 465 (calc. 467) cm^{-1}. The resonance Raman intensity of this mode is smaller than that of the symmetric C−N stretch that is observed at 1337 cm^{-1} (calc 1358 cm^{-1}), but its distortion is over twice as large because Δ_q scales as the square root of the intensity and the inverse square of the frequency. Distortions above 1.0 were also found for the low-frequency bending modes observed at 512, 605 and 750 cm^{-1}. The modes 1182 and 1268 cm^{-1} that involve aryl CN stretching also undergo rather large distortions ($\Delta_q = 0.77$ and 0.78, respectively). The mode at 1423 cm^{-1} involves NN stretching and that at 1581 cm^{-1} involves the aryl ring deformation.

One set of parameters was used to calculate the resonance Raman excitation profiles, the resonance Raman spectra at a given excitation wavelength, and the optical absorption spectrum.[25–28] The optical spectrum calculated is compared with the experimental one in Figure 4. Overlap of the higher energy component with the lower energy one at the excitation wavelengths studied for **2(Cl)**$^+$ was too large to make accurate calculations of the higher energy component, as was done in our previous work on **2(OMe)**$^+$.[10] A full-width at half-maximum (fwhm) of 5945 cm^{-1} for the lowest energy absorption was obtained, and the calculated and experimental spectra are in excellent agreement.

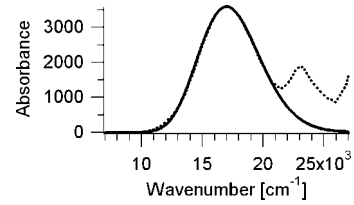

Figure 4. Calculated fit of the absorption spectrum of **2(Cl)**$^+$. The dotted line is the experimental spectrum at room temperature in acetronitrile, and the solid line is the calculated spectrum.

The Δ_q values given in Table 3 are dimensionless distortions. A commonly used way of providing more physical meaning to these distortions is to convert them to bond length changes, δ_q (Å), as shown in eq 1, where N_A is Avogadro's constant, $\hbar$ is Plank's constant in g cm^2 s^{-1}

$$\delta_q = 10^8 \Delta_q \sqrt{\frac{N_A \hbar}{2\pi\omega_q mc}} \quad (1)$$

divided by 2π, m is the normal mass of the vibration in molecular mass units, and c is the speed of light in cm s^{-1}. The normal masses were obtained from the UB3LYP/6-31G* calculation. A second way to more easily understand the significance of Δ values is to convert them to increments in λ_q^{sym} (cm^{-1}) using eq 2. Only symmetrical vibrations are enhanced in resonance

$$\lambda_q = 0.5\omega_q\Delta_q^2 \quad (2)$$

Raman spectra and contribute to the vibrational structure observed in absorption spectra. The λ_q^{sym} increments have a tendency to be larger relative to δ_q increments at higher vibrational energies. Figure 5 compares the λ_q^{sym} values for **2(Cl)**$^+$ obtained in the present work with those calculated from data reported previously for **2(H)**$^+$[9] and **2(OMe)**$^+$.[10] The total $\lambda_v^{sym} = \Sigma\lambda_q^{sym}$ values obtained increase substantially as the *p*-substituent lowers E_{a1}, in the order **2(H)**$^+$ (1400 cm^{-1}), **2(Cl)**$^+$ (5300 cm^{-1}), **2(OMe)**$^+$ (6000 cm^{-1}). We suggest that this trend occurs because more charge is transferred from the aryl groups to the **(NN)**$^{\bullet+}$ π system as the aryl group substituents lower the endothermicity of the electron transfer.

Discussion: Transition and Orbital Energy Calculations

The energy surfaces are shown in cartoon form in Figure 6 for **1(Cl)**$^{\bullet+}$ and **2(Cl)**$^{\bullet+}$. The simple excited state mixed valence

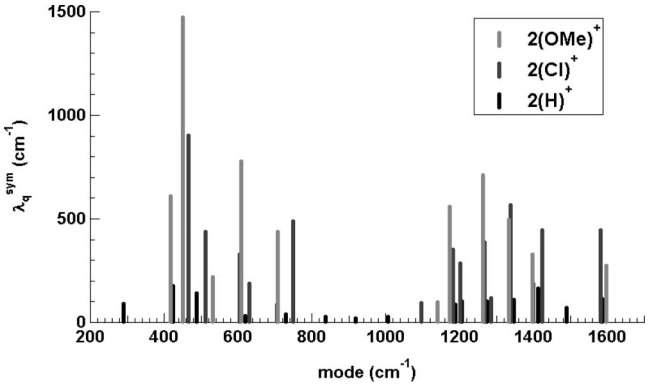

Figure 5. Comparison of λ_q^{syn} values from resonance Raman data.

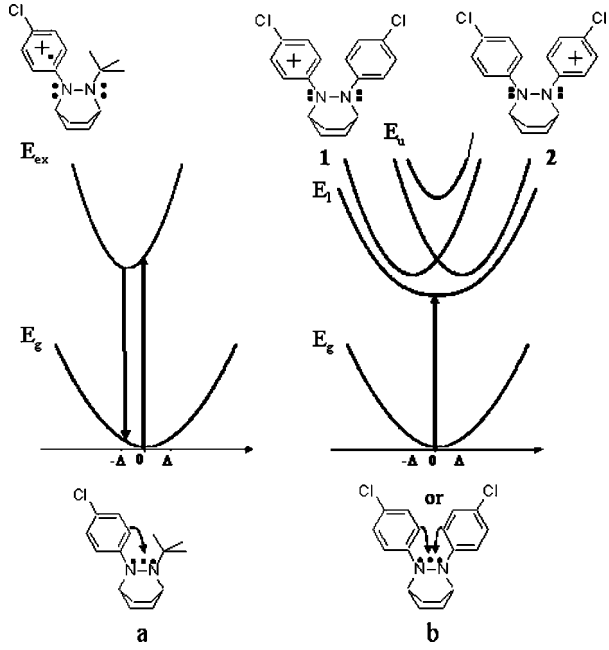

Figure 6. Ground and excited state potential energy surfaces for (a) chlorophenyl-to-$(NN)^+$ transition of **1(Cl)**$^{\bullet+}$. (b) The corresponding transitions of **2(Cl)**$^{\bullet+}$, where the excited state energy surface is split because of equivalent electron donation from the two chlorophenyl groups.

(ESMV) model shown includes a Marcus−Hush two-state diagram for the excited state. However, the minimum number of MOs necessary for quantitative consideration of the electronic couplings in **2(X)**$^{\bullet+}$ is actually four, as it is for delocalized MV diaminoaromatic radical cations[29] and dinitroaromatic radical anions,[30] for example. Four states are necessary because the two aryl rings produce symmetric and antisymmetric combination diabatic orbitals, and the symmetric and antisymmetric diabatic bridge orbitals (the symmetric $\pi(NN)^{\bullet+}$ and antisymmetric $\pi^*(NN)^{\bullet+}$ hydrazine orbitals for the present example) that have large overlaps and lie closest in energy to each will interact with them. These orbitals interact as independent Marcus−Hush two-state systems that share a common energy for the aryl group combination orbitals in the absence of direct overlap, as indicated in Figure 7, which we call a neighboring orbital diagram. Although in principle, all symmetric and antisymmetric MOs interact with each other separately, the $1/\Delta E$ relationship for the size of orbital interactions makes the smallest energy difference orbitals of high overlap interact the most. We consider next how the electronic interactions within **2**$^{\bullet+}$ are affected by tuning the energy of the aryl combination orbitals (**M**) relative to the $(NN)^{\bullet+}$ bridge by using substiutents **X** on

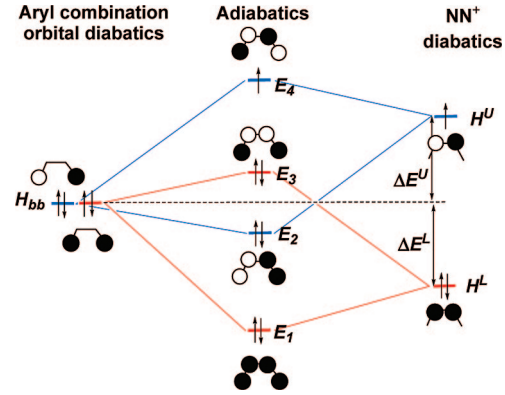

Figure 7. Neighboring orbital diagram for **2(X)**$^{\bullet+}$, simplifying the aryl ring π orbitals to single spots that represent symmetric and antisymmetric combinations of aryl π orbitals that interact with the π(NN) orbitals.

the aryl rings, and probe the effects on the MV transition using resonance Raman data for **2(Cl)**$^{\bullet+}$.

It is necessary to know the relative energies of the diabatic neighboring orbitals in Figure 7 to consider the electronic couplings H_{ab}. The experimental data most closely related to the relative energies of these orbitals are the transition energies, but because the orbital occupancy is different for the MOs involved in the transitions, one cannot simply compare calculated MO energies; the occupancy of an MO has a very large effect upon its calculated energy. We have calculated lower transition energies for **2(H)**$^+$, **2(Cl)**$^+$, and **2(OMe)**$^+$ using TD-DFT[31] at UB3LYP/6-31+G* optimized geometries using the Gaussian program,[32] and summarize the results in Table 4. Also included in Table 4 are the results of Koopmans-based neutral in cation geometry (NCG) calculations[33] that are employed in estimating the diabatic energies below. The transition energies are not what is required to estimate the diabatic energies, but the relative energies of the MOs relative to each other. When the MO that is the terminus of transitions is filled so that all of the orbitals involved are occupied by two electrons, the energy differences between the orbitals become realistic; they are not for the open-shell radical cation because of orbital occupancy differences. It is important to use the optimized geometry for the radical cation instead of that for the neutral compound when there is a large difference between the structures, as there is for hydrazines. Koopmans-based calculations do not attempt to include the configuration interaction that is present in variable amount in determining electronic transition energies. They estimate relative orbital energy differences between filled orbital and the singly occupied orbital (β to β-LUMO), called Hoijtink type A transitions,[34,35] using Koopmans' theorem,[36] that ionization potentials are the negative or orbital energies. As discussed in more detail elsewhere,[37–39] dication in cation geometry (DCG) calculations give transition energies for singly occupied orbital (α HOMO) to α virtual orbital, or Hoijtink type B transitions for radical cations. The MO energy differences for pure type A transitions can be obtained by calculations at the geometry of the radical cation but with a neutral charge, as the energy differences between the HOMO and the lower filled orbitals, whereas those for type B transitions may be obtained from a calculation of the dication at the radical cation geometry, as the energy difference between the LUMO and the higher unfilled orbitals. The intensities for both the type A and B transitions were calculated using Weinhold's NBO program as implemented in Gaussian.[40]

The two types of calculations are compared with the experimental absorption spectra of **2(H)**$^{\bullet+}$, **2(Cl)**$^{\bullet+}$, and

TABLE 4: B3LYP/6-31+G* Calculations of Optical Transitions

		TD-DFT			NCG/DCG	
2(X)$^{\bullet+}$	tr	$h\nu$(cm^{-1})[a]	f	TD assignment	$h\nu$(cm^{-1})[a]	f
H	1	17040	0.10	(93%) 70β →71β [A_1]	16460 A_1	0.06
(E_{a1} = 18000)	2	20920	0.01	(99%) 69β → 71β [A_2,π_x]	21540 A_2	0.01
	3	20970	0.00	(99%) 68α → 71α [A_3,π_x]	21650 A_3	0.00
	4	24810	0.04	(89%) 67β → 71β [A_4]	25320 A_4	0.06
	5	30700	0.02	17 transitions > 1%	33 880 B_1	0.04
Cl	1	14860	0.13	91% 86β → 87β [A_1]	14370 A_1	0.07
(E_{a1} = 17000)	2	20930	0.063	90% 85β → 87β [A_2] [a]	21480 A_2	0.06
	3	21870	0.008	99.4% 84β → 87β [A_3]	22360 A_3	0.01
	4	22380	0.009	96% 84β → 87β [A_4]	22950 A_4	0.01
	5	29170	0.022	18 transitions > 1%	31940 A_5	0.00
					31680 B_1	0.05
OMe	1	12950	0.13	(89%) 86β → 87β [A_1]	12340 A_1	0.07
(E_{a1} = 15200)	2	19770	0.08	(94%) 85β → 87β [A_2]	20130 A_2	0.07
	3	22700	0.01	(100%) 84β → 87β [A_3,π_x]	23370 A_3	0.01
	4	22800	0.00	(100%) 83β → 87β [A_4,π_x]	23510 A_4	0.00
	5	29350	0.01	16 transitions > 1%	30980 B_1	0.03

[a] Also 4% A_4, 2% B_1, 2% B_4, and 1% 86α → 89α (type C).

2(OMe)$^{\bullet+}$ in Figure 8. The TD-DFT calculations assign the transitions as nearly pure type A bands, so it is not surprising that the Koopmans-based method gives rather similar results to the TD-DFT calculations. For delocalized diaminoaromatic radical cations, which have small enough geometry reorganizations that vibrational fine structure is observed in the bands and the 0,0 band is the energy maximum, we found that the calculated band positions are several hundred to a few thousand wave numbers larger (for examples that involve considerable configuration interaction) than the observed 0,0 bands.[41] For **2(X)**$^{\bullet+}$, where the geometry reorganization is larger and the bands are broad and nearly Gaussian-shaped, the lower energy type A transitions are calculated by both methods to lie at lower in energies than those observed.

The higher energy occupied aryl MOs, which have the same energy in benzene, have one node through the aryl π system. Only the one with this node lying between the ortho and meta carbons has significant spin density at C_1, to which the nitrogen is attached, can mix with the **X** substituents and the hydrazine π system; we will designate this aryl MO as π_x. The aryl MO with its node passing through the NC_1 and C_4**X** bonds (π_y) has almost no interaction with either the hydrazine unit or the **X** substituents. This pair of noninteracting aryl rings in **2(X)**$^{\bullet+}$ gives rise to a pair of low intensity bands having similar energies; see Figure 8. They are calculated to have 50, 510, and 100 cm^{-1} separations, respectively, for **2(H)**$^{\bullet+}$, **2(Cl)**$^{\bullet+}$, and **2(OMe)**$^{\bullet+}$ using TD-DFT. Their average is centered at 20950 cm^{-1} for **2(H)**$^{\bullet+}$ (as A_2 and A_3), and at 22120 and 22700 cm^{-1}′for **2(Cl)**$^{\bullet+}$ and **2(OMe)**$^{\bullet+}$ (as A_3 and A_4), presumably higher in energy for the latter because of the σ electron-withdrawing effect of the heteroatomic aryl susbstituents. In contrast, the strongly mixed aryl MOs give rise to transitions with much larger oscillator strengths, and correspond to the two components observed for the split "mixed valence transition" of these compounds.

It will be noted in Figure 8 that although the TD-DFT and NCG/DCG calculations give rather similar transition energies, the intensities of the NCG/DCG calculations, which ignore effects of configuration interaction, do not behave properly as the substitutent **X** is changed, and those of the TD-DFT calculations are qualitatively better, predicting the observed increasing relative size of the higher energy component of the ESMV transition as the electron releasing power of the substitutent is increased.

Because very similar results are obtained using the less time-consuming 6-31G* instead of the larger 6-31+G* basis set, only the former are used for the rest of this paper. The relative orbital energies for **1(X)**$^{\bullet+}$ and **2(X)**$^{\bullet+}$ using the Koopmans-based NCG method with (U)B3LYP/6-31G* energies are summarized in Tables 5 and 6. All four of the neighboring orbitals of Figure 2 are shown in Table 6, but only the accuracy of the E_4-E_3 gap, which is the calculated first transition energy, is easily tested experimentally. We note that the $E_2 \rightarrow E_4$ transition is strongly forbidden and is not expected to be observed experimentally, and the $E_1 \rightarrow E_4$ transition is at high enough energy so that it will be obscured by stronger bands that have nothing to do with the N.O. system, so calculations are necessary to obtain couplings for Class III mixed valence compounds, which is a large difference from the usual assumption that a single two-state model can be used, which makes H_{ab} be half the transition energy. The problem with this simple assumption is that the MOs involved in the observed transition are of different symmetry, so that the transition cannot be arising from a single two-state model.

The effective orbital energies are obtained relative to the SOMO, which is the $\pi^*(NN)^+$ orbital for **1(X)**$^{\bullet+}$ and E_4 (see Figure 7) for **2(X)**$^{\bullet+}$. The first transition energies are compared with experiment in Figure 9, where it may be seen that the E_{a1} order **H** > **Cl** ≈ **Br** > **OMe** ≈ **Ph** is predicted correctly, and the mono- and diaryl compounds come close to lying on a single line. The calculated transition energies are significantly low, especially with electron-releasing substituents.

Neighboring Orbital Analysis

A neighboring orbital analysis was used to consider how the diabatic energies and thus the electronic couplings are affected by substituents. As discussed in detail elsewhere,[29,43] the two two-state systems that share a common energy (see Figure 7) allow estimating electronic couplings if an assumption is made about the relationship between electronic coupling and orbital energy differences; we use $V \propto \Delta E^{-1}$ relationship.

The diabatic energies are obtained as a function of the difference between the diabatic energy of the π_y aryl combination orbitals (H_{bb}) and the bonding NN^+ π orbital (H^L), $\Delta E^L = H_{bb} - H^L$ (shown in Figure 1) are shown graphically for **2(X)**$^{\bullet+}$ in Figure 10. The entire range of real solutions to the N.O. equations is shown. The plots for the other compounds are

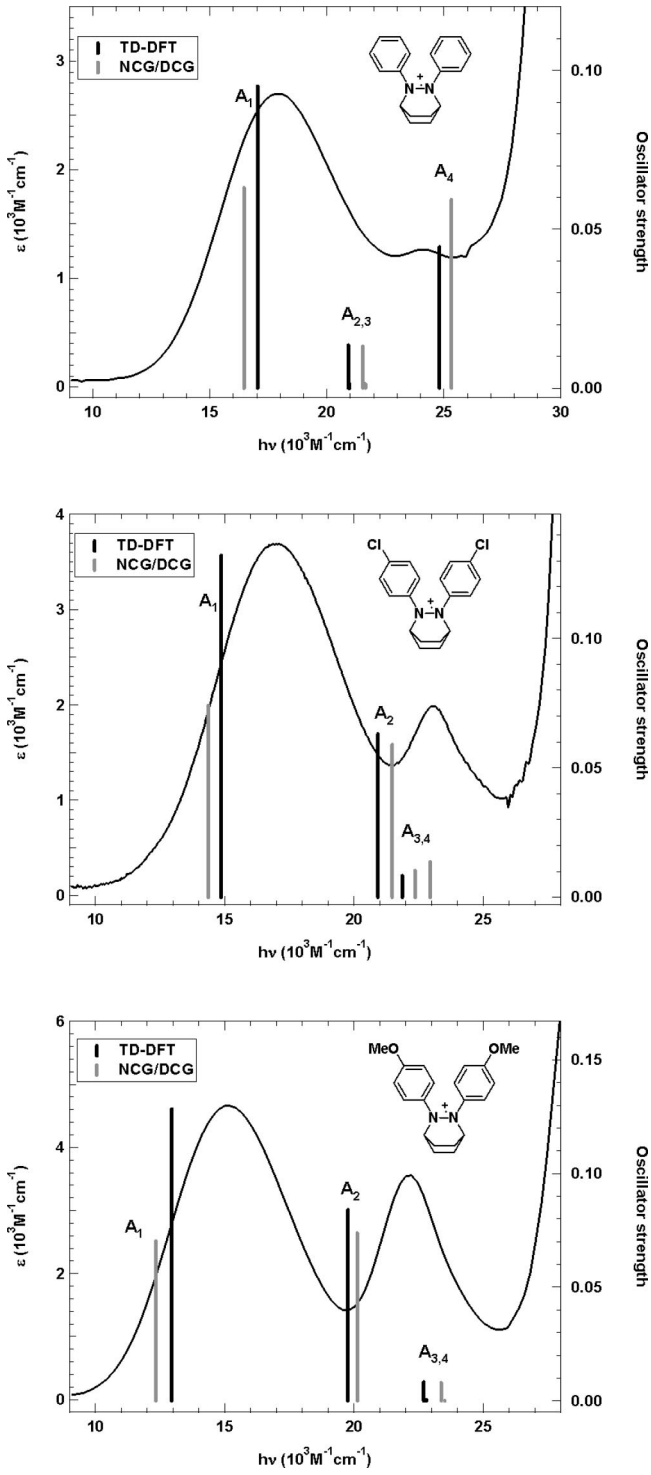

Figure 8. Comparison of TD-DFT (red) and Koopmans-based calculations with optical spectra for **2(H)**$^{\bullet+}$ (top panel), **2(Cl)**$^{\bullet+}$ (middle panel), and **2(OMe)**$^{\bullet+}$ (bottom panel).

similar; see the Supporting Information. The H_{bb} line is displaced upward relative to the parallel H^{U} and H^{L} lines with increasingly electron-releasing substituents, and it has almost the same energy as H^{U} at the high ΔE^{L} limit for **2(NMe$_2$)**$^{\bullet+}$. H_{bb} is displaced downward so it is even closer to H^{L} at the lower ΔE^{L} limit for **2(NO$_2$)**$^{\bullet+}$. Assuming a $1/\Delta E$ dependence for electronic interactions causes the plots shown in Figure 10 for **2(H)**$^{\bullet+}$. V^{L} is larger than V^{U} when H_{bb} is closer to H^{L}, and vice versa. The ratio $R = \Delta E^{U}V^{L}/\Delta E^{U}V^{U}$ is also shown in Figure 10 (on the right vertical axis). We expect the correct solution to the N.O. problem

TABLE 5: (U)B3LYP/6-31G* Calculated Effective Orbital Energies for 1(X)$^{\bullet+}$

X	calc E_{a1}	calc − obs E_{a1}	ΔE ($\pi_x - \pi_y$)
NMe$_2$	12280		11390
OMe	17620	1980	8020
Ph	17690	1810	6670[a]
Br	20580	1120	5520
Cl	20820	880	5230
H	22610	−110	2150
NO$_2$	23460		1650

[a] Using the average of the biphenyl π_x values, which differ by 220 cm^{-1}.

to have R reasonably close to 1; that is, the proportionality constants for $V = \text{constant}/\Delta E$ will be about the same size. R does not have to be exactly 1 because of overlap effects, but how to treat such effects quantitatively is complicated,[44] and we do not attempt it here. The sensitivity of R to ΔE^{L} varies greatly at different points within the allowed ΔE^{L} range. It is very sensitive at the edges and insensitive in the middle. R suddenly goes to $-\infty$ and $+\infty$ at the ends because $H_{ab}{}^{L} \rightarrow 0$ at the left edge, and $H_{ab}{}^{U} \rightarrow 0$ at the right edge of the plots. R for **2(H)**$^{+}$ is very sensitive to ΔE^{L} near $R = 1$ (at the extreme left of Figure 10), which we argue is the correct solution as indicated by the trend of substituent effects and the position of the noninteracting π_y orbitals,[41] so the calculated V values, especially the larger V^{L}, are rather well determined for these compounds. These considerations lead to the orbital pictures of Figure 11 for **2(H)**$^{+}$.[45] Note that the aryl π_x orbital combinations (H_{bb}) become properly destabilized relative to the noninteracting π_y orbitals using these $R = 1$ solutions.

Although it is true that the symmetric and antisymmetric combinations of the aryl group orbitals will not have exactly the same energy because of direct overlap of their π systems, we present calculations relating to the size of this overlap effect on the N.O. analysis in the Supporting Information, because the effects calculated on both the diabatic energies and the electronic couplings are small. We therefore only show the results calculated at $\Delta H_{bb} = 0$ in Table 7, which summarizes the calculations of diabatic energies and electronic couplings as a function of substituent.

The diabatic energies from Table 7 are plotted versus the Taft σ_{R+} value in Figure 12, which represents the resonance electron-releasing ability of substituents, and is obtained from ^{19}F NMR chemical shifts of meta- and para-substituted fluorobenzenes.[10] The reasonable correlation is consistent with the N.O. analysis producing reasonable diabatic orbital energies. The diabatic aryl π_y combination orbital energy H_{bb} is calculated to be stabilized in the expected order by over 10000 cm^{-1} (28.6 kcal/mol) as the p-substituent is changed from NMe$_2$ to NO$_2$, but the effect on the larger electronic coupling, V_L, is estimated to be largest for the H-substituted compound, and to only drop by about 1100 cm^{-1} over this series. The energy difference between H_{bb} and the noninteracting π_x orbitals of the diaryl compounds **2(X)**$^{\bullet+}$ is calculated to change by 12550 cm^{-1} by the N.O. analysis (last column of Table 7), whereas the $\pi_y - \pi_x$ energy difference changes for the monoaryl compounds **1(X)**$^{\bullet+}$ by 9740 cm^{-1} for the same substituent change (last column of Table 6).

Conclusions

Although **2(Cl)** is harder to oxidize to the radical cation than **2(H)** and **2(OMe)** is easier, the NN and NAr twist angles and nitrogen pyramidality calculated for **2(Cl)**$^{\bullet+}$ lie between those

TABLE 6: (U)B3LYP/6-31G* Calculated Effective Orbital Energies for 2(X)$^{\bullet+}$ [a]

X	E_4	E_3	E_2	E_1	calc − obs E_{a1}	$E_{av}(\pi_x)$ [$\Delta E(\pi_x)$]
NMe_2	0	−7786	−15550	−26782		−22884 [449]
OMe	0	−12130	−19770	−32446	3070	−22532 [787]
		−12340[b]	−20130[b]	−32400[b]	2860[b]	−23440 [140][b]
Ph	0	−11307	−16633	−22729	3690	−20126 [307]
Cl	0	−14380	−21503	−32003	2620	−22569 [565]
Br	0	−14062	−20478	−29314	2940	−22328 [410]
H	0	−16450	−25351	−36001	1550	−21561 [64]
		−16460[b]	−25320[b]	−36000[b]	1540[b]	−21445 [110][b]
NO_2	0	−16920	−25629	−35401	480	−21000 [465]
$(NO_2)_2$	0	−20830	−27080	−35684	6830	−23736 [465]

[a] Calculated using Spartan.[42] [b] Results of 6/31+G* calculations.

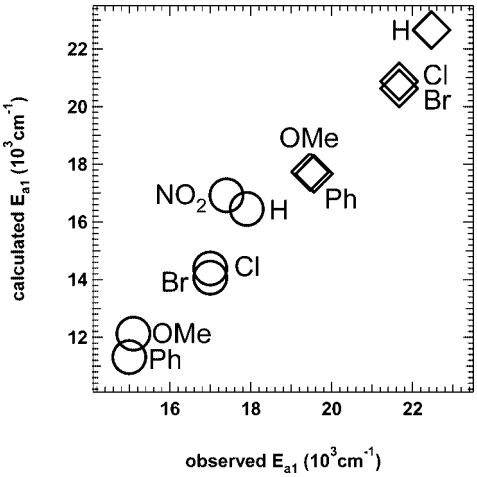

Figure 9. Plot of calculated versus observed first transition energies for **2(X)**$^{\bullet+}$ (circles) and **1(X)**$^{\bullet+}$ (diamonds).

for **2(H)**$^{\bullet+}$ and **2(OMe)**$^{\bullet+}$, demonstrating that the *p*-chlorophenyl aryl group stabilizes the $(NN)^+$-centered radical cation better than a phenyl group. **2(Cl)**$^{\bullet+}$ also has a transition energy and ε_{max} value between those for **2(OMe)**$^{\bullet+}$ and **2(H)**$^{\bullet+}$, so the C_6H_4Cl stabilizes the electron transfer transition to the $\pi^*(NN)^{\bullet+}$-centered SOMO better than C_6H_5. The same trend is shown by the increase in reorganization energy for symmetric vibrations, λ_v^{sym}, determined by resonance Raman spectroscopy, which increases from 1400 cm^{-1} for **2(H)**$^{\bullet+}$ to 5300 cm^{-1} for **2(Cl)**$^{\bullet+}$ and 6000 cm^{-1} for **2(OMe)**$^{\bullet+}$. The neighboring orbital analysis of the Koopmans-based calculations of relative adiabatic energies demonstrates that the larger electronic coupling is that to the more stabilized, filled π(NN) orbital, (V^L), which is on the order of 9200 ± 600 cm^{-1} and is not calculated to vary regularly with electron-releasing power of the substituent. The $E_3 - E_2$ energy gap, which is the energy difference between the two components of the mixed valence transition, and which we have referred to as the "effective electronic coupling" when using the simpler excited state mixed valence model,[11,12] is determined by the differences in all three diabatic energies, as well as both V^U and V^L.[10]

Experimental Section

1. Synthesis. 2-*tert*-Butyl-3-(4-chlorophenyl)-2,3-diazabicyclo[2.2.2]octane, 1(Cl), was prepared by the same method as 1(OMe),[12] with 4-chlorobromobenzene substituted for 4-bromoanisole. Mp: 75−76 °C. ^{1}H NMR: (CD_2Cl_2) δ 7.75 (d, J = 8.6 Hz, 1H), 7.10 (d, J = 8.6 Hz, 1H), 7.08 (d, J = 9.0 Hz, 1H), 6.89 (d, J = 9.0 Hz, 1H), 3.67 (s, 1H), 3.34 (s, 1H), 2.23−1.2 (m, 8H), 1.07 (s, 9H). Empirical formula $C_{16}H_{23}ClN_2$ established by high resolution mass spectrometry.

2-*tert*-Butyl-3-(4-bromophenyl)-2,3-diazabicyclo[2.2.2]octane, 1(Br), was prepared by the same method as 1(OMe),[12] with 1,4-dibromobenzene substituted for 4-bromoanisole. Mp: 82−83 °C. ^{1}H NMR: (CD_3CN) δ 8.08 (d, J = 8.3 Hz, 1H), 7.64 (m, 2H), 7.21 (d, J = 10.0 Hz, 1H), 4.05 (s, 1H), 3.82 (s, 1H), 2.6−1.5 (m, 8H), 1.46 (s, 9H). Empirical formula $C_{16}H_{23}BrN_2$ established by high resolution mass spectrometry.

2-*tert*-Butyl-3-(4-iodophenyl)-2,3-diazabicyclo[2.2.2]octane, 1(I), was prepared by the same method as 1(OMe),[12] with 1,4-diiodobenzene substituted for 4-bromoanisole. Mp: 85−86 °C. ^{1}H NMR: (CD_3CN) δ 8.06 (d, J = 8.1 Hz, 1H), 7.61 (m, 2H), 7.21 (d, J = 9.0 Hz, 1H), 4.02 (s, 1H), 3.70 (s, 1H), 2.6−1.5 (m, 8H), 1.46 (s, 9H). Empirical formula $C_{16}H_{23}IN_2$ established by high resolution mass spectrometry.

2-*tert*-Butyl-3-(4-biphenylyl)-2,3-diazabicyclo[2.2.2]octane, 1(Ph), was prepared by the same method as 1(OMe),[12] with 4-bromobiphenyl substituted for 4-bromoanisole. Mp: 77−78 °C. ^{1}H NMR: (CD_3CN) δ 7.9−7.0 (m, 9H), 3.8 (s, 1H), 3.4 (s, 1H), 2.0−1.2 (m, 8H), 1.10 (s, 9H). Empirical formula $C_{22}H_{28}N_2$ established by high resolution mass spectrometry.

2-*tert*-Butyl-3-(4-nitrophenyl)-2,3-diazabicyclo[2.2.2]octane, 1(NO_2). Into a 100 mL Schlenk flask containg 60 mL of dry ether and 0.11 g (1 mmol) of 2,3-diazabicyclo[2.2.2]oct-2-ene was added 1 mmol (0.6 mL of a 1.7 mM solution in pentane) of *tert*-butyllithium at −78 °C under nitrogen. After 1 h at −78 °C, 0.155 g (1.1 mmol) of 1-fluoro-4-nitrobenzene was added. After warming to room temperature, cold water was added, the organic layer was separated, and the aqueous layer was extracted with ether. The organic solution was dried over magnesium sulfate, solvents were removed under reduced pressure, and the reisdue was crystallized from methanol/ether to give 0.12 g (42%) of **1(NO_2)**. Mp: 119−120 °C. ^{1}H NMR: (CD_3CN) δ 8.05 (m, 2H), 7.87 (d, J = 8.9 Hz, 1H), 6.97 (d, J = 9.0 Hz, 1H), 4.00 (s, 1H), 3.45 (s, 1H), 2.6−1.5 (m, 8H), 1.14 (s, 9H). The empirical formula $C_{16}H_{23}N_3O_2$ was established by high resolution mass spectroscopy.

2-*tert*-Butyl-3-(4-cyanophenyl)-2,3-diazabicyclo[2.2.2]octane, 1(CN), was made by the same method as **1(NO_2)**, substituting 4-fluorocyanobenzene for 4-fluoronitrobenzene. Mp: 128−129 °C. ^{1}H NMR: ($CDCl_3$) δ 7.70 (m, 2H), 7.08 (m, 2H), 3.52, (s, 1H), 3.48 (s, 1H), 2.25−1.27 (m, 8H), 1.23 (s, 9H). The empirical formula $C_{17}H_{23}N_3$ was established by high resolution mass spectroscopy.

2,3-Bis(4-chlorphenyl)-2,3-diazabicyclo[2.2.2]octane, 2(Cl), was prepared as in the published route for its 2,3-dianisyl analogue,[12] except that 4-chlorobromobenzene replaced 4-bromoanisole. Mp: 156−157 °C. ^{1}H NMR ($CDCl_3$) δ 7.18 (d, J - 9.0 Hz, 4H), 687 (d, J - 9.0 Hz, 4H), 4.10 (s, 2H); 1.45−2.2 (complex, 8H); ^{13}C NMR (CD_3CN) δ 149.2, 128.8, 124.1, 115.8,

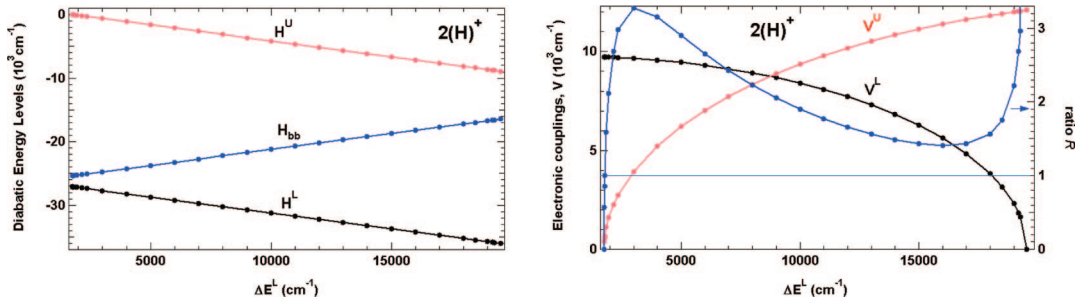

Figure 10. (Left panel) Plot of the diabatic energies of **22/Ph$_2$**$^+$ obtained in a neighboring orbital analysis as a function of ΔE^L. (Right panel) plot of the N.O. electronic couplings (left axis) and their ratio $R = V^L/V^U$ as a function of ΔE^L.

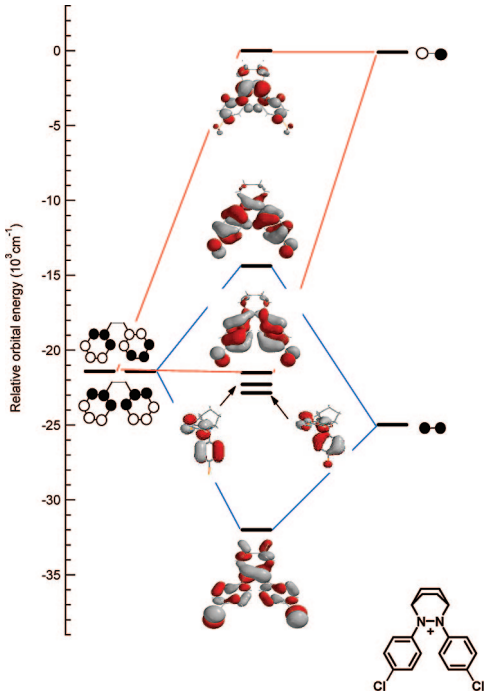

Figure 11. Neighboring orbital diagrams for **2(Cl)**$^{\bullet+}$. Similar diagrams for the **X = H**, **OMe**, **NMe$_2$** and **NO$_2$** substituted compounds are shown in Supporting Information.

TABLE 7: Neighboring Orbital Analysis at $R = 1$ for (U)B3LYP/6-31G* Calculations on 2(X)$^{\bullet+}$, at $\Delta H_{bb} = 0$

substituent	H_{bb}	H^U	H^L	V^U	V^L	$H_{bb} - E_{av}(\pi_x)$
NMe$_2$[a]	−14950	−600	−19620	3000	9210	7930
OMe[a]	−19260	--510	−25310	3130	9700	3270
Cl	−21410	−100	−24980	1450	8630	2760
H	−25330	−20	−27120	690	9740	−3770
NO$_2$	−25620	−5	−26600	350	9280	−4620

[a] See ref 44.

48.6, 24.8, 19.7. The empirical formula $C_{18}H_{18}Cl_2N_2$ was established by high resolution mass spectrometry.

2,3-Bis(4-bromophenyl)-2,3-diazabicyclo[2.2.2]octane, 2(Br), was prepared as in the published route for its 2,3-dianisyl analogue,[12] except that 1.4-dibromobenzene replaced 4-bromoanisole, and the ratio of dibromobenzene to *tert*-butyllithium employed was 1.0:0.95. Mp: 164−165 °C. ^{1}H NMR ($CDCl_3$) δ 7.51 (d, $J = 8.9$ Hz, 4H), 6.79 (d, $J = 8.9$ Hz, 4H), 4.08 (s, 2H), 2.2−1.5 (m, 8H). The empirical formula $C_{18}H_{18}Br_2N_2$ was established by high resolution mass spectrometry.

2,3-Bis(4-iodophenyl)-2,3-diazabicyclo[2.2.2]octane, 2(I), was prepared as in the published route for its 2,3-dianisyl analogue,[12] except that 1,4-diiodobenzene replaced 4-bromoanisole. Mp: 184−185 °C. ^{1}H NMR ($CDCl_3$) δ 7.46 (d, $J = 9.1$ Hz, 4H), 6.71 (d, $J = 9.1$ Hz, 4H), 4.07 (s, 2H), 2.2−1.5 (m, 8H). The empirical formula $C_{18}H_{18}I_2N_2$ was established by high resolution mass spectrometry.

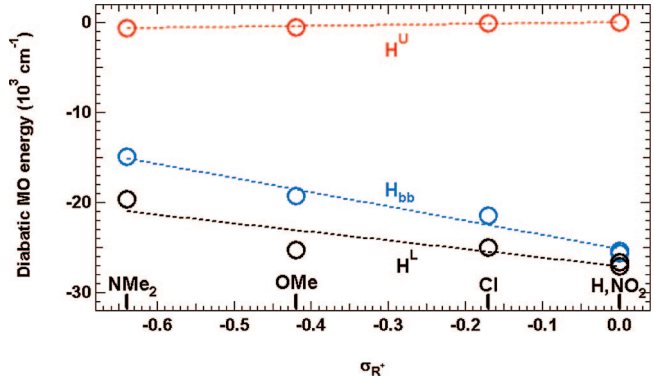

Figure 12. Plot of the diabatic energies for **2(X)**$^+$ from Table 7 versus σ_{R+}.

2,3-Bis(4-biphenylyl)-2,3-diazabicyclo[2.2.2]octane, 2(Ph), was prepared as in the published route for its 2,3-dianisyl analogue,[10] except that 4-bromobiphenyl replaced 4-bromoanisole. Mp: 242−243 °C. ^{1}H NMR ($CDCl_3$) δ 7.8−6.9 (m, 18H), 4.15 (s, 2H), 2.2−1.45 (m, 8H). The empirical formula $C_{30}H_{28}N_2$ was established by high resolution mass spectrometry.

2,3-Bis(4-nitrophenyl)-2,3-diazabicyclo[2.2.2]octane, 2(NO$_2$), was prepared by nitration of 2-phenyl-3-(4-nitrophenyl)-2,3-diazabicyclo[2.2.2]octane, which was prepared by the method of Neugebauer and Weger.[46] A solution of 0.2 g (6.1 mmol) of the mononitrated compound in 10 mL of acetic aced was treated dropwise with a solution of 0.5 mL of concentrated nitric acid in 10 mL of acetic acid. A 60 mL quantity of ice water was added 1 min after the addition was complete. After filtering, washing with water, air drying, and crystallization from an ether/methanol mixture, 0.19 (87.2%) of **2(NO$_2$)**, mp 229−230 °C, was obtained. ^{1}H NMR ($CDCl_3$) δ 8.10 (d, $J = 10$ Hz, 4H), 7.27 (d, $J = 10$ Hz, 4H), 4.35 (s, 2H), 2.2−1.45 (m, 8H). The empirical formula $C_{18}H_{18}N_4O_4$ was established by high resolution mass spectrometry.

2,3-Bis(2,4-dinitrophenyl)-2,3-diazabicyclo[2.2.2]octane, 2(NO$_2$)$_2$ was prepared by the same method as **2 (NO$_2$)**, but an excess of concentrated nitric acid was employed. Mp: 201−202 °C. ^{1}H NMR ($CDCl_3$) δ 8.73(d, J=2.5 Hz, 2H), 8.34 (dd, $J = 9.0$,2.5 Hz, 2H), 8.13, (d, $J = 9.0$ Hz, 2H), 3.74 (s, 2H), 1.5−2.2 (m, 8H).

2,3-Bis(4-cyanophenyl)-2,3-diazabicyclo[2.2.2]octane, 2(CN), was prepared almost quantitatively by refluxing 2(Br) or 2(I) with 4.0 equiv of $(CuCN)_2$ for 24 h in dimethylformamide. Mp: 230−231 °C. ^{1}H NMR ($CDCl_3$) δ 7.43 (d, $J = 8.5$ Hz, 4H), 6.83 (d, $J = 9.0$ Hz, 4H), 4.17 (s, 2H), 2.1−1.5 (m, 8H). The empirical formula $C_{20}H_{18}N_4$ was established by high resolution mass spectrometry.

2. Absorption spectra were taken at room temperature using acetronitrile solution samples generated by oxidation with tris(*p*-bromophenyl)aminium antimony hexachloride. Solid oxidant (about 8.1 mg, 11.28 mmol) and hydrazine (in slight excess, about 12.0 mmol) were diluted to 25.00 mL in a volumetric flask with freshly dried acetonitrile, and 1 mL of solution was transferred to a 10 mL volumetric flask and diluted to 10.00 mL, giving a 45 μM solution.

3. Raman spectra of 2(Cl)$^+$ were obtained using a 1401 Spex double monochromator equipped with a Burle C31034 photomultiplier tube and a Stanford Research Systems SR400 photon counter, and by using an ISA triple monochromator with a CCD. Excitation was provided by an argon ion laser (for wavelength of 514.5 nm) and a krypton ion laser (for wavelengths of 482.5, 568.2, 647.1 and 676.4 nm). Spectra were collected from acetronitrile solutions contained in capillary tubes made from a solvent matrix mixture of **2(Cl)$^{\bullet+}$** and acetronitrile as reference at a molar concentration of 3×10^{-3} M. The intensities were obtained by numerically integrating the peaks. The Raman intensities were normalized to that of the acetronitrile standard. The absorption and Raman spectra were analyzed as described in our previous work.[9,10]

Acknowledgment. This work was made possible by grants from the National Science Foundation, CHE-0507929 (JIZ), CHE-0240197 and -0647719 (SFN), CONACyT 43226, DGAPA-UNAM IN111902, and UCMEXUS Grant Collaboration. S.F.N. acknowledges gifts from the Intel Corporation and grant CHE0091916 from the NSF for support of the departmental computers used in this work. G.V.A. is grateful for a UC-MEXUS-CONACYT postdoctoral fellowship.

Supporting Information Available: Full Gaussian citations, spectra of **2(Ph)**$^+$ and **2(NO$_2$)**$^+$, and **2(NO$_2$)$_2$**$^+$, Raman spectra of **2(Cl)**$^+$ with 568 and 488 nm excitation, N.O. equations and energy plots for **2(NMe$_2$)**$^+$, **2(OMe)**$^+$, **2(Cl)**$^+$, **2(NO$_2$)**$^+$, and **2(NO$_2$)$_2$**$^+$, N.O. MO plots for **2(H)**$^+$, **2(OMe)**$^+$, **2(NMe$_2$)**$^+$, and **2(NO$_2$)**$^+$, and discussion of the effect of direct overlap of the aryl groups on calculated parameters. This material is available free of charge via the Internet at http://pubs.acs.org.

References and Notes

(1) Robin, M. B.; Day, P. *Adv. Inorg. Radiochem.* **1967**, *10*, 247.
(2) (a) Nelsen, S. F. *Acc. Chem. Res.* **1981**, *14*, 131. (b) Nelsen, S. F.; Liebman, J. F.; Greenberg, A. *Molecular Structures and Energetics*; VCH Publishers, Inc.: Deerfield Beach, FL, 1986, Vol. 3,
(3) Creutz, C. *Prog. Inorg. Chem.* **1983**, *30*, 1.
(4) (a) Broo, A.; Larsson, S. *Chem. Phys.* **1990**, *148*, 103. (b) Braga, M.; Broo, A.; Larsson, S. *Chem. Phys.* **1991**, *156*, 1.
(5) Brunschwig, B. S.; Creutz, C.; Sutin, N. *Chem. Soc. Rev.* **2002**, *31*, 168.
(6) Demadis, K. D.; Hartshorn, C. M.; Meyer, T. J. *Chem. Rev.* **2001**, *101*, 2655.
(7) Nelsen, S. F. *Chem. Eur. J.* **2000**, *6*, 581.
(8) Lockard, J. V.; Zink, J. I.; Trieber, D. A. II; Konradsson, A. E.; Weaver, M. N.; Nelsen, S. F. *Chem. Phys.* **2006**, *324*, 195.
(9) Lockard, J. V.; Zink, J. I.; Trieber, D. A.; Konradsson, A. E.; Weaver, M. N.; Nelsen, S. F. *J. Phys. Chem. A* **2005**, *109*, 1205.
(10) Lockard, J. V.; Valverde, G.; Neuhauser, D.; Zink, J. I.; Luo, Y.; Weaver, M. N.; Nelsen, S. F. *J. Phys. Chem. A* **2006**, *110*, 57.
(11) Hansch, C.; Leo, A.; Taft, R. W. *Chem. Rev.* **1991**, *91*, 165.
(12) Adam, W.; Harrer, H. M.; Kita, F.; Korth, H.-G.; Nau, W. M. *J. Org. Chem.* **1997**, *62*, 1419.
(13) Nau, W. M.; Harrer, H. M.; Adam, W. *J. Am. Chem. Soc.* **1994**, *116*, 10972.
(14) Claridge, R. F. C.; Fischer, H. *J. Phys. Chem.* **1983**, *87*, 1960.
(15) Lee, S.-Y.; Heller, E. J. *J. Chem. Phys.* **1979**, *71*, 4777.
(16) Heller, E. J. *Acc. Chem. Res.* **1981**, *14*, 368.
(17) Heller, E. J.; Sundberg, R. L.; Tannor, D. *J. Phys. Chem.* **1982**, *86*, 1822.
(18) Myers, A. B. *Laser Techniques in Chemistry*; Wiley: New York, 1995.
(19) Myers Kelley, A. *J. Phys. Chem. A* **1999**, *103*, 6891.
(20) Myers, A. B. *Chem. Rev.* **1996**, *96*, 911.
(21) Myers, A. B. *Acc. Chem. Res.* **1997**, *30*, 519.
(22) Zink, J. I.; Shin, K.-S. K. *Advances in Photochemistry*; Wiley: New York, 1991; Vol. 16, p 119.
(23) Shin, K.-S. K.; Zink, J. I. *Inorg. Chem.* **1989**, *28*, 4358.
(24) Shin, K, K. -S.; Zink, J. I. *J. Am. Chem. Soc.* **1990**, *112*, 7148.
(25) Wootton, J. L.; Zink, J. I. *J. Am. Chem. Soc.* **1997**, *119*, 1895.
(26) Wootton, J. L.; Zink, J. I. *J. Phys. Chem.* **1995**, *99*, 7251.
(27) Reber, C.; Zink, J. I. *J. Phys. Chem.* **1991**, *95*, 9151.
(28) Henary, M.; Zink, J. I. *J. Am. Chem. Soc.* **1989**, *111*, 7407.
(29) Nelsen, S. F.; Luo, Y.; Weaver, M. N.; Lockard, J. V.; Zink, J. I. *J. Org. Chem.* **2006**, *71*, 4286.
(30) (a) Nelsen, S. F.; Konradsson, A. E.; Weaver, M. N.; Telo, J. P. *J. Am. Chem. Soc.* **2003**, *125*, 12493. (b) Nelsen, S. F.; Weaver, M. N.; Telo, J. P.; Zink, J. I. *J. Am. Chem. Soc.* **2005**, *127*, 10611.
(31) (a) Burke, K.; Gross, E. K. U. In *Density Functionals:Theory and Applications*; Joubert, D., Ed.; Springer: Berlin, 1998; pp 116−146. (b) Casida, M. E.; Jamorski, C.; Casida, K. C.; Salhub, D. R. *J. Chem. Phys.* **1998**, *108*, 4439. (c) Stratmann, R. E.; Scuseria, G. E.; Frisch, M. J. *J. Chem. Phys. Chem.* **1998**, *109*, 8218–8224.
(32) (a) Frisch, M. J.; et. al. *Gaussian 98*, revision A.9; Gaussian, Inc.: Pittsburgh, PA, 1998. (b) Frisch, M. J.; et. al. *Gaussian 03*, revision B.05; Gaussian, Inc., Pittsburgh, PA, 2003.
(33) Nelsen, S. F.; Blackstock, S. C.; Yumibe, N. P.; Frigo, T. B.; Carpenter, J. E.; Weinhold, F. *J. Am. Chem. Soc.* **1985**, *107*, 143.
(34) Bally, T.; Lund, A.; Shiotani, M. *Radical Ionic Systems*; Kluwer: Dortrecht, The Netherlands, 1991, p 3.
(35) (a) Hoijtink, G. J.; Weijland, W. P. *Recl. Trav. Chim.* **1957**, *76*, 836. (b) Buschow, K. J. J.; Dieleman, J.; Hoijtink, G. J. *Mol. Phys.* **1963**, 1964.
(36) Koopmans, T. *Physica* **1933**, *1*, 104.
(37) Nelsen, S. F.; Weaver, M. N.; Telo, J. P.; Zink, J. I. *J. Am. Chem. Soc.* **2005**, *127*, 10611.
(38) Nelsen, S. F.; Weaver, M. N.; Telo, J. P.; Lucht, B. L.; Barlow, S. *J. Org. Chem.* **2005**, *70*, 9326.
(39) Nelsen, S. F.; Weaver, M N.; Bally, T.; Yamazaki, D.; Komatsu, K.; Rathore, R. *J. Phys. Chem. A* **2007**, *111*, 1667.
(40) NBO 5.0. E. D. Glendening, J. K. Badenhoop, A. E. Reed, J. E. Carpenter, J. A. Bohmann, C. M. Morales, and F. Weinhold (Theoretical Chemistry Institute, University of Wisconsin, Madison, WI, 2001).
(41) Nelsen, S. F.; Luo, Y.; Weaver, M. N.; Lockard, J. V.; Zink, J. I. *J. Org. Chem.* **2006**, *71*, 4286.
(42) Spartan '02, Wavefunction Inc., Irvine, CA.
(43) Nelsen, S. F.; Weaver, M. N.; Luo, Y.; Lockard, J. V.; Zink, J. I. *Chem. Phys.* **2006**, *324*, 195.
(44) For discussion in the context of the ethane rotational barrier problem, see: Weinhold, F. *Angew. Chemie Int. Ed.* **2003**, *42*, 4188–4194.
(45) Although there are three $R = 1$ solutions for **2(OMe)**$^+$ and **2(NMe2)**$^+$, and R gets rather close to 1 in the high ΔE^L region for the other compounds, only the smallest ΔE^L solutions place the π_x orbital energies in the proper relation to the other energies for these compounds.
(46) Neugebauer, F. A.; Weger, H. *Chem. Ber.* **1979**, *112*, 1076.

JP7120005